Trajectory Tracking Control of Autonomous Underwater Vehicles Using Improved Tube-Based Model Predictive Control Approach

Li-Ying Hao, *Member, IEEE*, Run-Zhi Wang, Chao Shen, *Member, IEEE*, and Yang Shi, *Fellow, IEEE*

***Abstract*—This article aims to develop a robust model predictive control (MPC) scheme for the trajectory tracking control of autonomous underwater vehicles (AUVs) subject to bounded disturbances. Based on the error dynamics model derived from the AUV dynamics and the desired trajectory, an improved tube-based MPC scheme is then developed. The tube-based MPC solves two optimal control problems, the first solves a standard problem for the nominal system which defines a reference state trajectory, and the other attempts to steer the state of the disturbed system to stay in a tube centered around the reference state trajectory thereby enabling robust control of the AUV systems. For tube-based nonlinear MPC, finding a local linear feedback to characterize the tube is challenging. To address it, we replace the local linear feedback controller with an ancillary one that incorporates the tightening constraints to ensure the disturbed system state stays in the online optimized tube. The simulation results demonstrate the effectiveness of the proposed method.**

***Index Terms*—Autonomous underwater vehicles (AUVs), nonlinear model predictive control, robust model predictive control (MPC), trajectory tracking, tube-based model predictive control.**

I. Introduction

THE usefulness of autonomous underwater vehicles (AUVs) is increasingly apparent due to the expanding exploration and exploitation of the oceans [1], [2]. AUVs present an efficient, intelligent, and fully autonomous means to sense, monitor, and interact with the marine environment. Throughout the last few decades, many control techniques have been developed to address the trajectory tracking issue, such as the line-of-sight scheme [3], PID control [4], linear quadratic Gaussian control [5], and sliding-mode technique [6]. For the planar motion control of AUVs, a nonlinear controller was presented in [7] by adopting the Lyapunov direct approach and backstepping methodology. Nevertheless, the above control techniques applied to AUVs lack the ability to handle system constraints, which are inescapable, such as state constraint and actuator limits. Fortunately, model predictive control (MPC) [8], [9], [10] is an excellent algorithm that can handle constraints, which prompts researchers to apply MPC to solve the trajectory tracking problem of AUVs. Shi and Zhang [11] provided a comprehensive overview of the application of MPC in autonomous intelligent mechatronic systems. In [12], the AUV model was linearized, and then the trajectory tracking control was carried out on the linearized model. Linear MPC is highly effective at solving convex optimization problems, and when coupled with acceleration algorithms [13], [14], it can achieve real-time control. However, linearizing a system can result in model mismatch, and some nonlinear systems cannot be linearized directly. In response to this challenge, research on nonlinear MPC has become crucial. In [15], the stabilizing conditions of tracking control for nonlinear AUVs were explicitly addressed for the first time. Additionally, in [16], a Lyapunov-based MPC (LMPC) framework was developed for AUVs, aiming to leverage computational resources to improve tracking performance. In [17], a stochastic MPC approach was proposed by integrating the concept of stochastic control Lyapunov-barrier function. To address the challenge of the high computational burden associated with nonlinear MPC, a highly efficient algorithm was proposed in [18].

In real-world applications, disturbances and uncertainties are inevitable, which results in a mismatch in the relationship between the predicted and actual state in MPC control strategies. Robustness has thus been of great interest in the MPC community [19], [20], [21]. Due to the receding-horizon implementation, standard MPC enables the feedback control and hence has

Manuscript received 17 August 2023; revised 27 September 2023; accepted 27 October 2023. Date of publication 11 December 2023; date of current version 4 April 2024. This work was supported in part by the National Natural Science Foundation of China under Grant 52171292 and Grant 51939001, in part by the Outstanding Young Talent Program of Dalian under Grant 2022RJ05, and in part by National Sciences and Engineering Research Council of Canada under Grant RGPIN-2022-04940 and Grant DGECR-2022-00106. Paper no. TII-23-3145. *(Corresponding authors: Li-Ying Hao; Yang Shi.)*

Li-Ying Hao and Run-Zhi Wang are with the Marine Electrical Engineering College, Dalian Maritime University, Dalian 116026, China (e-mail: haoliying_0305@163.com; wangrz1220@163.com).

Chao Shen is with the Department of System and Computer Engineering, Carleton University, Ottawa, ON K1S 5B6, Canada (e-mail: shenchao@sce.carleton.ca).

Yang Shi is with the Department of Mechanical Engineering, University of Victoria, Victoria, BC V8P 5C2, Canada (e-mail: yshi@uvic.ca).

Color versions of one or more figures in this article are available at https://doi.org/10.1109/TII.2023.3331772.

Digital Object Identifier 10.1109/TII.2023.3331772

certain degrees of inherent robustness against sufficiently small uncertainties and disturbances [22], [23], [24]. Nevertheless, standard MPC may be incapable of meeting performance specifications in actual AUV applications subject to large disturbances and uncertainty. There has been significant research dedicated to developing robust MPC techniques tailored for autonomous marine vehicles. In [25], a robust control framework for AUVs was developed to facilitate LMPC-based trajectory tracking. The LMPC leverages the inherent stability and robustness offered by the auxiliary control law based on the extended state observer. In [26], a constraint tightening technique was employed for the tracking control of underwater robotic vehicles. This approach ensures that the nominal system's state constraints are sufficiently tight, thereby guaranteeing the admissibility of the real system's evolution throughout the entire time horizon. A tube-based MPC approach could be found in [27], utilizing a linearized model of an autonomous surface vehicle. It should be mentioned that tube-based MPC has been extensively studied due to its advantages of having similar complexity as standard MPC and less conservative closed-loop performance [11]. By incorporating local feedback control laws, the main goal is to maintain all feasible states in a tube. Designing a feedback law to generate a robust invariant set for nonlinear versions of tube-based MPC is typically an intractable problem. In [28], the incremental Lyapunov function's sublevel sets were utilized to describe the tube. The inclusion of predicted dimensions of the tube as scalar variables in optimization problems was proposed in [29]. In [30] and [31], the local linear feedback has been replaced with an auxiliary MPC controller. The tube was defined by the optimal value of the cost function, providing a bound on the system's behavior. However, obtaining an explicit characterization of the tubes through cost functions proved to be challenging. To address it, we utilize an auxiliary controller that incorporates tightened constraints related to the tube to optimize the size of an explicitly expressed tube. The main contributions of this article can be explained from the following perspectives.

1) Different from the existing literature [30], [31], in which no explicit characterization of tubes is given, we have established the shape of the tube offline and optimized the parameters of the tube online, providing a clear understanding of its properties. Furthermore, we have adjusted the initial feasible set.
2) A class of ancillary controller is proposed to replace the linear feedback one in traditional tube-based MPC. The ancillary controller incorporates the tube-related tightening constraints, and the cost function includes parameters of the tube as decision variables.
3) The improved MPC scheme guarantees the feasibility of the MPC problem when the system state is given within the initial set. It has been proven that the AUV system's input-to-state stability (ISS) is maintained in the presence of bounded disturbances.

The rest of this article is organized as follows. Section II introduces the AUV's nonlinear dynamics and kinematics model. An error dynamics model is derived from the AUV dynamics and the reference trajectory. Section III describes the problem formulation according to the proposed controller. In Section IV, the proposed tube-based MPC algorithm is detailed. The parameter selection and the track performance under the tube-based robust MPC are represented in Section V. Finally, Section VI concludes the article.

Notation: The superscripts "-1" and "T" denote the matrix inverse and the matrix transposition, respectively. The function atan2$(\cdot,\cdot)$ denotes the four-quadrant arctangent function. For a column vector x and a matrix P with appropriate dimensions, $\|x\|$ represents the Euclidean norm of x, and $\|x\|_P$ represents the P-weighted norm of x. For a given matrix Q, $Q>0$ indicates that the matrix Q is positive definite, while $R\geq 0$ implies that the matrix R is positive semidefinite. The symbol diag$(\cdot)$ represents a diagonal matrix.

II. AUV Model

A. Dynamic and Kinematic Model

The dynamic equation of AUV motion [15] can be expressed as

$$\mathbf{M}\dot{\mathbf{v}}+\mathbf{C}(\mathbf{v})\mathbf{v}+\mathbf{D}(\mathbf{v})\mathbf{v}+\mathbf{g}(\boldsymbol{\eta})=\boldsymbol{\tau} \tag{1}$$

where $\mathbf{M}=\text{diag}(M_x,M_y,M_\psi)$ represents the inertia matrix, $\mathbf{v}$ denotes AUV's surge, sway, and yaw velocity vector, specifically expressed as $\mathbf{v}=\begin{bmatrix}u & v & r\end{bmatrix}^{\mathrm{T}}$, and $\boldsymbol{\eta}$ denotes AUV's position and orientation vector, specifically expressed as $\boldsymbol{\eta}=\begin{bmatrix}x & y & \psi\end{bmatrix}^{\mathrm{T}}$. $\mathbf{C}(\mathbf{v})$ is Coriolis and centripetal matrix, specifically expressed as

$$\mathbf{C}(\mathbf{v})=\begin{bmatrix}0 & 0 & -M_y v\\ 0 & 0 & M_x u\\ M_y v & -M_x u & 0\end{bmatrix}.$$

$\mathbf{D}(\mathbf{v})=\text{diag}(X_u+D_u|u|,Y_v+D_v|v|,N_r+D_r|r|)$ is damping matrix, $\mathbf{g}(\boldsymbol{\eta})$ represents restoring force, in this article, $\mathbf{g}(\boldsymbol{\eta})=\mathbf{0}$, and $\boldsymbol{\tau}=\begin{bmatrix}F_u & F_v & F_r\end{bmatrix}^{\mathrm{T}}$ represents all of the forces and moments acting on the vehicle. Details of other symbols can be found in Section V and the literature [15].

The expansion of the dynamic (1) can be expressed as follows:

$$\begin{aligned}\dot{u}&=\frac{M_y}{M_x}ur-\frac{X_u}{M_x}u-\frac{D_u}{M_x}u|u|+\frac{F_u}{M_x},\\ \dot{v}&=\frac{M_x}{M_y}vr-\frac{Y_v}{M_y}v-\frac{D_v}{M_y}v|v|+\frac{F_v}{M_y},\\ \dot{r}&=\frac{M_x-M_y}{M_\psi}uv-\frac{N_r}{M_\psi}r-\frac{D_r}{M_\psi}r|r|+\frac{F_r}{M_\psi}.\end{aligned} \tag{2}$$

The AUV kinematic equation can be formulated as

$$\dot{\boldsymbol{\eta}}=\begin{bmatrix}\cos\psi & -\sin\psi & 0\\ \sin\psi & \cos\psi & 0\\ 0 & 0 & 1\end{bmatrix}\begin{bmatrix}u\\ v\\ r\end{bmatrix}\triangleq R(\psi)\mathbf{v}. \tag{3}$$

Consider $\boldsymbol{\tau}$ to be the generalized control input, and consider $\mathbf{x}\triangleq\text{col}(\boldsymbol{\eta},\mathbf{v})$ to be the generalized system state. The AUV model is derived from (1) and (3).

$$\dot{\mathbf{x}}=\begin{bmatrix}\mathbf{R}(\psi)\mathbf{v}\\ \mathbf{M}^{-1}(\boldsymbol{\tau}-\mathbf{C}(\mathbf{v})-\mathbf{D}(\mathbf{v})-\mathbf{g}(\boldsymbol{\eta}))\end{bmatrix}\triangleq\mathbf{f}(\mathbf{x},\boldsymbol{\tau}). \tag{4}$$

B. Error Dynamics Model

The desired path to be tracked is denoted by $p_m = \begin{bmatrix} x_m & y_m \end{bmatrix}^{\mathrm{T}}$. We assume that p_m is third differentiable. From the desired path p_m, we can calculate the desired AUV states $\psi_m = \text{atan2}(\dot{y}_m, \dot{x}_m)$, $u_m = \sqrt{\dot{x}_m^2 + \dot{y}_m^2}$, $v_m = 0$ and $r_m = \dot{\psi}_m$. $\mathbf{v}_m \triangleq \begin{bmatrix} u_m & v_m & r_m \end{bmatrix}^{\mathrm{T}}$.

In the AUV parallel reference structure [1], the kinematic error $\boldsymbol{\eta}_e$ can be developed as

$$\boldsymbol{\eta}_e = \begin{bmatrix} x_e \\ y_e \\ \psi_e \end{bmatrix} = \begin{bmatrix} \cos\psi & \sin\psi & 0 \\ -\sin\psi & \cos\psi & 0 \\ 0 & 0 & 1 \end{bmatrix} \begin{bmatrix} x_m - x \\ y_m - y \\ \psi_m - \psi \end{bmatrix}. \quad (5)$$

We can express the velocity error as $\mathbf{v}_e = \mathbf{v} - R(\psi_e)\mathbf{v}_m$, where $\mathbf{v}_e = \begin{bmatrix} u_e & v_e & r_e \end{bmatrix}^{\mathrm{T}}$. The kinematic error equation are obtained by differentiating (5) and substituting (1) and (3)

$$\begin{aligned} \dot{x}_e &= -u_e + y_e r_e + y_e r_m, \\ \dot{y}_e &= -v_e - x_e r_e - x_e r_m, \\ \dot{\psi}_e &= -r_e. \end{aligned} \quad (6)$$

Expand $\mathbf{v}_e = \mathbf{v} - R(\psi_e)\mathbf{v}_m$ into an element-wise expression

$$\begin{aligned} u_e &= u - u_m \cos\psi_e + v_m \sin\psi_e, \\ v_e &= v - u_m \sin\psi_e - v_m \cos\psi_e, \\ r_e &= r - r_m. \end{aligned} \quad (7)$$

We take the derivative of both sides of $\mathbf{v}_e = \mathbf{v} - R(\psi_e)\mathbf{v}_m$

$$\begin{aligned} \dot{u}_e &= \dot{u} - \dot{u}_m \cos\psi_e - u_m \sin\psi_e r_e + \dot{v}_m \sin\psi_e - v_m \cos\psi_e r_e, \\ \dot{v}_e &= \dot{v} - \dot{u}_m \sin\psi_e + u_m \cos\psi_e r_e - \dot{v}_m \cos\psi_e - v_m \sin\psi_e r_e, \\ \dot{r}_e &= \dot{r} - \dot{r}_m. \end{aligned} \quad (8)$$

Substituting (2) into (8), we have

$$\begin{aligned} \dot{u}_e = {} & \frac{M_y}{M_x}(v_e + u_m \sin\psi_e + v_m \cos\psi_e)(r_e + r_m) - \frac{X_u}{M_x} \\ & (u_e + u_m \cos\psi_e - v_m \sin\psi_e) - \frac{D_u}{M_x}(u_e + u_m \cos\psi_e \\ & - v_m \sin\psi_e)|u_e + u_m \cos\psi_e - v_m \sin\psi_e| - \dot{u}_m \cos\psi_e \\ & - u_m \sin\psi_e r_e + \dot{v}_m \sin\psi_e - v_m \cos\psi_e r_e + \frac{F_u}{M_x}, \\ \dot{v}_e = {} & -\frac{M_x}{M_y}(u_e + u_m \cos\psi_e - v_m \sin\psi_e)(r_e + r_m) - \frac{Y_u}{M_y} \\ & (v_e + u_m \sin\psi_e + v_m \cos\psi_e) - \frac{D_v}{M_y}(v_e + u_m \sin\psi_e \\ & + v_m \cos\psi_e)|v_e + u_m \sin\psi_e + v_m \cos\psi_e| - \dot{u}_m \sin\psi_e \\ & + u_m \cos\psi_e r_e - \dot{v}_m \cos\psi_e - v_m \sin\psi_e r_e + \frac{F_v}{M_y}, \\ \dot{r}_e = {} & \frac{M_x - M_y}{M_\psi}(u_e + u_m \cos\psi_e - v_m \sin\psi_e)(v_e + u_m \sin\psi_e \\ & + v_m \cos\psi_e) - \frac{N_r}{M_\psi}(r_e + r_m) \\ & - \frac{D_r}{M_\psi}(r_e + r_m)|r_e + r_m| - \dot{r}_m + \frac{F_r}{M_\psi}. \end{aligned} \quad (9)$$

By utilizing (9), we can derive a detailed design for F_u, F_v, and F_r

$$\begin{aligned} F_u = {} & -M_y(v_e + u_m \sin\psi_e + v_m \cos\psi_e)(r_e + r_m) + X_u(u_e \\ & + u_m \cos\psi_e - v_m \sin\psi_e) \\ & + D_u(u_e + u_m \cos\psi_e - v_m \sin\psi_e) \\ & |u_e + u_m \cos\psi_e - v_m \sin\psi_e| + M_x(\dot{u}_m \cos\psi_e \\ & + u_m \sin\psi_e r_e - \dot{v}_m \sin\psi_e + v_m \cos\psi_e r_e) + M_x V_u, \\ F_v = {} & M_x(u_e + u_m \cos\psi_e - v_m \sin\psi_e)(r_e + r_m) + Y_v(v_e \\ & + u_m \sin\psi_e + v_m \cos\psi_e) \\ & + D_v(v_e + u_m \sin\psi_e + v_m \cos\psi_e) \\ & |v_e + u_m \sin\psi_e + v_m \cos\psi_e| \\ & + M_y(\dot{u}_m \sin\psi_e - u_m \cos\psi_e r_e \\ & + \dot{v}_m \cos\psi_e + v_m \sin\psi_e r_e) + M_y V_v, \\ F_r = {} & (M_x - M_y)(u_e + u_m \cos\psi_e - v_m \sin\psi_e)(v_e + u_m \sin\psi_e \\ & + v_m \cos\psi_e) + N_r(r_e + r_m) + D_r(r_e + r_m)|r_e + r_m| \\ & + M_\psi \dot{r}_m + M_\psi V_r. \end{aligned} \quad (10)$$

By defining the input $V_e = \begin{bmatrix} V_u & V_v & V_r \end{bmatrix}^{\mathrm{T}}$ of the error model and substituting (10) into (9), together with (6), we can get the nominal error dynamics model, as shown below

$$\dot{Z}_e = \begin{bmatrix} \dot{x}_e \\ \dot{y}_e \\ \dot{\psi}_e \\ \dot{u}_e \\ \dot{v}_e \\ \dot{r}_e \end{bmatrix} = \begin{bmatrix} -u_e + y_e r_e + y_e r_m \\ -v_e - x_e r_e - x_e r_m \\ -r_e \\ V_u \\ V_v \\ V_r \end{bmatrix} = f_e(Z_e, V_e). \quad (11)$$

For the nominal AUV system, there are certain input constraints. Although the control input does not directly affect the system, it will influence the generation of the nominal trajectory. $\bar{\omega} = \begin{bmatrix} \bar{\omega}_u & \bar{\omega}_v & \bar{\omega}_r \end{bmatrix}^{\mathrm{T}}$ represents the upper bound of disturbances. Detailed descriptions can be found in Section III. The specific constraints on the control input are as follows:

$$\begin{aligned} F_u &\in [F_{u,\min} - \bar{\omega}_u, F_{u,\max} - \bar{\omega}_u], \\ F_v &\in [F_{v,\min} - \bar{\omega}_v, F_{v,\max} - \bar{\omega}_v], \\ F_r &\in [F_{r,\min} - \bar{\omega}_r, F_{r,\max} - \bar{\omega}_r]. \end{aligned} \quad (12)$$

Through (12), the input constraint $\mathbb{V}_e$ of the error system (11) is obtained

$$V_u \in \left[\frac{F_{u,\min} - F_1 - \bar{\omega}_u}{M_x}, \frac{F_{u,\max} - F_1 - \bar{\omega}_u}{M_x} \right],$$

$$V_v \in \left[\frac{F_{v,\min}-F_2-\bar{\omega}_v}{M_y}, \frac{F_{v,\max}-F_2-\bar{\omega}_v}{M_y}\right],$$
$$V_r \in \left[\frac{F_{r,\min}-F_3-\bar{\omega}_r}{M_\psi}, \frac{F_{r,\max}-F_3-\bar{\omega}_r}{M_\psi}\right] \quad (13)$$

where the explicit expressions of $F_1 = F_u - M_x V_u, F_2 = F_v - M_y V_v, F_3 = F_r - M_\psi V_r$ in (10).

If the error system (11) exhibits asymptotic stability, the state of the error system will eventually reach equilibrium point $(\mathbf{0}, \mathbf{0})$, which implies that the position error $\boldsymbol{\eta}_e$ and velocity $\mathbf{v}_e$ are both zero. Consequently, the system has successfully tracked the desired path.

III. Problem Formulation

In real applications, the existence of disturbances is inevitable. Disturbances can occur for many reasons, such as waves and wind. We incorporate the disturbances into the dynamic equations of motion

$$\mathbf{M}\dot{\mathbf{v}} + \mathbf{C}(\mathbf{v})\mathbf{v} + \mathbf{D}(\mathbf{v})\mathbf{v} + \mathbf{g}(\boldsymbol{\eta}) = \boldsymbol{\tau} + \omega \quad (14)$$

where $\omega = \begin{bmatrix}\omega_u & \omega_v & \omega_r\end{bmatrix}^{\mathrm{T}} \in \mathbb{W}$, $\mathbb{W}$ represents a disturbance set. This implies that the disturbances are bounded. Specifically, an upper bound for disturbances is denoted as $\bar{\omega} = \begin{bmatrix}\bar{\omega}_u & \bar{\omega}_v & \bar{\omega}_r\end{bmatrix}^{\mathrm{T}}$. Thus, the AUV model can be written as follows with explicit consideration for disturbances:

$$\dot{\mathbf{x}} = \begin{bmatrix}\mathbf{R}(\psi)\mathbf{v} \\ \mathbf{M}^{-1}(\boldsymbol{\tau} + \omega - \mathbf{C}(\mathbf{v}) - \mathbf{D}(\mathbf{v}) - \mathbf{g}(\boldsymbol{\eta}))\end{bmatrix} = \mathbf{f}(\mathbf{x}, \boldsymbol{\tau}, \omega). \quad (15)$$

Substituting (14) into (8), we have

$$\dot{\tilde{X}}_e = \begin{bmatrix}\dot{\tilde{x}}_e \\ \dot{\tilde{y}}_e \\ \dot{\tilde{\psi}}_e \\ \dot{\tilde{u}}_e \\ \dot{\tilde{v}}_e \\ \dot{\tilde{r}}_e\end{bmatrix} = \begin{bmatrix}-\tilde{u}_e + \tilde{y}_e\tilde{r}_e + \tilde{y}_e\tilde{r}_d \\ -\tilde{v}_e - \tilde{x}_e\tilde{r}_e - \tilde{x}_e\tilde{r}_d \\ -\tilde{r}_e \\ U_u + \frac{\omega_u}{M_x} \\ U_v + \frac{\omega_v}{M_y} \\ U_r + \frac{\omega_r}{M_\psi}\end{bmatrix} = f_e(\tilde{X}_e, U_e, \omega). \quad (16)$$

For the disturbed AUV system, there are limits to real actuators. The specific constraints on the control input are as follows:

$$\tilde{F}_u \in [F_{u,\min}, F_{u,\max}],$$
$$\tilde{F}_v \in [F_{v,\min}, F_{v,\max}],$$
$$\tilde{F}_r \in [F_{r,\min}, F_{r,\max}]. \quad (17)$$

Through (10), the input constraint $\mathbb{U}_e$ of the error system (16) is obtained

$$U_u \in \left[\frac{F_{u,\min}-\tilde{F}_1}{M_x}, \frac{F_{u,\max}-\tilde{F}_1}{M_x}\right],$$
$$U_v \in \left[\frac{F_{v,\min}-\tilde{F}_2}{M_y}, \frac{F_{v,\max}-\tilde{F}_2}{M_y}\right],$$
$$U_r \in \left[\frac{F_{r,\min}-\tilde{F}_3}{M_\psi}, \frac{F_{r,\max}-\tilde{F}_3}{M_\psi}\right]. \quad (18)$$

Specifically, (10) is modified by replacing $V_e = \begin{bmatrix}V_u & V_v & V_r\end{bmatrix}^{\mathrm{T}}$ with $U_e = \begin{bmatrix}U_u & U_v & U_r\end{bmatrix}^{\mathrm{T}}$, resulting in the expressions $\tilde{F}_1 = \tilde{F}_u - M_x U_u$, $\tilde{F}_2 = \tilde{F}_v - M_y U_v$, and $\tilde{F}_3 = \tilde{F}_r - M_\psi U_r$.

Remark 1: For a more concise representation, we introduce a scaling factor α such that $\mathbb{V}_e = \alpha\mathbb{U}_e$. α is inversely related to $\bar{\omega}$. The selection of α should meet the requirements specified in (12), (13), (17), and (18). It is advisable to choose $\mathbb{V}_e$ to be slightly conservative, but excessively small values may impact the size of the optimization problem's attraction domain. Conversely, if $\mathbb{V}_e$ is too large, it may lead to violations of input constraints in Problem 2 due to disturbances. Striking a balance between conservatism and feasibility is crucial to ensuring the effectiveness of the approach.

IV. Tube-Based MPC

In this section, a tube-based nonlinear MPC strategy is developed. The controller is split into two components: 1) a nominal MPC controller which calculates the reference trajectory of system (11) by discarding the disturbances in the AUV dynamics; and 2) an ancillary MPC controller that keep the disturbed system state near to the calculated nominal trajectory.

A. Nominal MPC Controller

The reference trajectory is obtained by addressing nominal optimization problems that drive the nominal system (11) to track the desired path p_m from the initial state $Z_e(0) = X_e(0)$. The reference trajectory $Z_e(t), t \in (0, \infty)$ is generated through *Problem* 1. The cost function of this nominal optimization problem $J_1(t, Z_e(t), V_e(t))$ has the following definition:

$$J_1(t, Z_e(t), V_e(t)) = h(Z_e(t+T_1)) + \int_t^{t+T_1} l(Z_e(s), V_e(s))ds \quad (19)$$

where $T_1 = N_1\delta$, δ is the sampling interval, N_1 is the prediction horizon, $h(Z_e) = \frac{1}{2}Z_e^T Z_e$ is the terminal cost, see [15] for details. The stage cost is expressed as $l(Z_e, V_e) = Z_e^{\mathrm{T}} Q Z_e + V_e^{\mathrm{T}} R V_e$, where $Q > 0$ and $R \geq 0$.

Problem 1: Given the current error state $Z_e(t_0)$, the proposed nominal optimization problem is as follows:

$$\min_{V_e} \quad J_1(t_0, Z_e(t_0), V_e(t_0)) \quad (20)$$
$$\text{s.t.} \quad \dot{Z}_e(t) = f_e(Z_e(t), V_e(t)),\ t \in [t_0,\ t_0 + T_1] \quad (21)$$
$$Z_e(t) \in \mathbb{Z}_e,\ t \in [t_0,\ t_0 + T_1] \quad (22)$$
$$V_e(t) \in \mathbb{V}_e,\ t \in [t_0,\ t_0 + T_1] \quad (23)$$
$$Z_e(t_0 + T_1) \in \mathbb{Z}_f \quad (24)$$

where $\mathbb{Z}_e = \{Z_e \| \|Z_e\| \leq \varsigma\}, \varsigma > 0$ represents a feasible region, $\mathbb{V}_e$ is an input constraint, as detailed in (13). $\mathbb{Z}_f = \{Z_e \| \|Z_e\| \leq \sigma\}, \sigma > 0$, is the terminal constraint, as detailed in [15].

Solving *Problem* 1 yields $\bar{Z}_e(t),\ t \in [t_0,\ t_0+T_1]$ as the optimal state trajectory. The initial moment of $\bar{V}_e(t)$ serves as the control input $\bar{\kappa}_N(t)$ for the nominal system. In other words, $\bar{\kappa}_N(t) = \bar{V}_e(t), t \in [t_0,\ t_0+\delta]$. The closed-loop nominal system is established as follows:

$$\dot{Z}_e(t) = f_e(Z_e(t), \bar{\kappa}_N(t)). \tag{25}$$

Theorem 1: Assuming the conditions $A1, A2$, and $A3$ are achieved, the asymptotic stability of the nominal closed-loop system (25) is guaranteed.

A1: $\mathbf{0} \in \mathbb{Z}_f$ and $\mathbf{0} \in \mathbb{V}_e$.
A2: A local controller V_e^L exists and satisfies

a) $V_e^L \in \mathbb{V}_e$, for all $Z_e \in \mathbb{Z}_f$.
b) $f_e(Z_e, V_e^L) \in \mathbb{Z}_f$, for all $Z_e \in \mathbb{Z}_f$.
c) $\dot{h}(Z_e) + l(Z_e, V_e^L) \leq 0$ for all $Z_e \in \mathbb{Z}_f$.

A3: $\bar{V}_e(t|t_0)$ represents the optimal control sequence for solving Problem 1 at time t_0. Based on the $\bar{V}_e(t|t_0)$, a candidate control input sequence $\hat{V}_e(t|t_0+\delta)$ at $t_0+\delta$ is selected as follows:

$$\hat{V}_e(t|t_0+\delta) = \begin{cases} \bar{V}_e(t|t_0) & t \in [t_0,\ t_0+T_1) \\ V_e^L & t \in [t_0+T_1,\ t_0+T_1+\delta]. \end{cases} \tag{26}$$

Proof: The optimal value J_1^0 of (19) is selected as Lyapunov function candidate. $\bar{V}_e(t|t_0)$ represents the optimal control input calculated by solving *Problem* 1 at time t_0 and the associated state sequence $\bar{Z}_e(t|t_0)$. $\hat{V}_e(t|t_0+\delta)$, $\hat{Z}_e(t|t_0+\delta)$, and $\hat{J}_1^0(t_0+\delta, Z_e(t_0+\delta))$ represents the candidate control input sequence (26) at time $t_0+\delta$, the corresponding optimal trajectory and the corresponding optimal cost function, respectively. Clearly, $\hat{V}_e(t|t_0+\delta)$ is a suboptimal control input sequence, which implies that $J_1^0(t_0+\delta, Z_e(t_0+\delta)) \leq \hat{J}_1(t_0+\delta, Z_e(t_0+\delta))$. Consider the variation in the Lyapunov function between t_0 and $t_0+\delta$

$$\begin{aligned} &J_1^0(t_0+\delta, Z_e(t_0+\delta)) - J_1^0(t_0, Z_e(t_0)) \qquad (27)\\ &\leq \hat{J}_1(t_0+\delta, Z_e(t_0+\delta) - J_1^0(t_0, Z_e(t_0)\\ &\leq J_1(t_0+\delta, \hat{Z}_e(t_0+\delta), \hat{V}_e(t_0+\delta)) - J_1(t_0, \bar{Z}_e(t_0), \bar{V}_e(t_0))\\ &\leq h(\hat{Z}_e(t_0+\delta+T_1)) - h(\bar{Z}_e(t_0+T_1))\\ &\quad + \int_{t_0+\delta}^{t_0+\delta+T_1} l(\hat{Z}_e(s|t_0+\delta), \hat{V}_e(s|t_0+\delta))ds\\ &\quad - \int_{t_0}^{t_0+T_1} l(\bar{Z}_e(s|t_0), \bar{V}_e(s|t_0)ds. \qquad (28) \end{aligned}$$

With regard to (26), we can see that for $s \in [t_0+\delta,\ t_0+T_1]$, $\hat{Z}_e(s|t_0+\delta) = \bar{Z}_e(s|t_0)$, $\hat{V}_e(s|t_0+\delta) = \bar{V}_e(s|t_0)$, thus we have

$$\begin{aligned} &J_1^0(t_0+\delta, Z_e(t_0+\delta)) - J_1^0(t_0, Z_e(t_0))\\ &\leq h(\hat{Z}_e(t_0+\delta+T_1))\\ &\quad + \int_{t_0+T_1}^{t_0+\delta+T_1} l(\hat{Z}_e(s|t_0+\delta), \hat{V}_e(s|t_0+\delta))ds\\ &\quad - h(\bar{Z}_e(t_0+T_1)) - \int_{t_0}^{t_0+\delta} l(\bar{Z}_e(s|t_0), \bar{V}_e(s|t_0)ds. \end{aligned}$$

Given that $\dot{h}(\hat{Z}_e) + l(\hat{Z}_e, \hat{V}_e) \leq 0$, we can integrate both sides of t_0+T_1 to get $t_0+\delta+T_1$, then

$$\begin{aligned} &h(\hat{Z}_e(t_0+\delta+T_1)) - h(\hat{Z}_e(\delta+T_1))\\ &\quad + \int_{t_0+T_1}^{t_0+T_1+\delta} l(\hat{Z}_e(s|t_0+\delta), \hat{V}_e(s|t_0+\delta))ds \leq 0. \end{aligned}$$

Hence we have

$$\begin{aligned} &J_1^0(t_0+\delta, Z_e(t_0+\delta)) - J_1^0(t_0, Z_e(t_0))\\ &\leq -\int_{t_0}^{t_0+\delta} l(\bar{Z}_e(s|t_0), \bar{V}_e(s|t_0))ds \leq 0. \end{aligned}$$

The function $l(\cdot,\cdot)$ is quadratic and positive definite, implying that $J_1^0(t_0+\delta, Z_e(t_0+\delta)) - J_1^0(t_0, Z_e(t_0)) \leq 0$. Solving *Problem* 1 ensures that the system (11) asymptotically approaches the equilibrium point $(\mathbf{0}, \mathbf{0})$. ■

We define the reference state trajectory $Z_e^*(t)$ to be the solution of the closed-loop system (25) whose associated input is $V_e^*(t) \triangleq \kappa_N(t)$. It is noteworthy that in order to solve for $V_e^*(t)$ and $Z_e^*(t)$, there are numerous operations needed, which are detrimental to the whole process. In order to make computations simpler, the reference state sequences $Z_e^*(t)$ and reference input sequences $V_e^*(t)$ can be redefined as: Taking the minimizing control sequences $\bar{V}_e(t)$ and associated optimal state sequences $\bar{Z}_e(t)$ solved by *Problem* 1 as reference state sequences $Z_e^*(t)$ and reference input sequences $V_e^*(t)$, respectively. The reference redefinition can greatly simplify the computation, but at the same time it puts an limit on the prediction horizon of the ancillary controller.

Remark 2: The modification of the initial feasible set $\mathbb{Z}_e$ is in comparison to the methodology described in [16]. In our approach, the feasibility domain is determined by *Problem* 1, which is based on the framework from [16]. However, we have extended this concept by introducing more restrictive input constraints, as elaborated in (13). Consequently, the size and definition of the feasibility domain in our work deviate from those in [16].

B. Ancillary MPC Controller

For tube-based nonlinear MPC, it is difficult to find a local linear feedback to characterize the tube. Consequently, in this article, we substitute the local linear feedback with an ancillary controller. An ancillary optimization problem that seeks to minimize the distance among the nominal system (11) and the disturbed system (16) is solved to produce an implicit control law. As illustrated in Fig. 1, the tube is defined as

$$T_d(t, \bar{Z}_e(t), S(t)) = \{\tilde{X}_e(t) | \|\tilde{X}_e(t) - \bar{Z}_e(t)\|_{\bar{Q}} \leq S(t)\} \tag{29}$$

where $\tilde{X}_e(t)$ represents the disturbed state, and $X_e(t)$ represents the predicted state determined by *Problem* 2, $\bar{Q}$ describes the shape of the tube, $S(t)$ represents the tube-size, $\dot{S}(t) = \gamma(t)$.

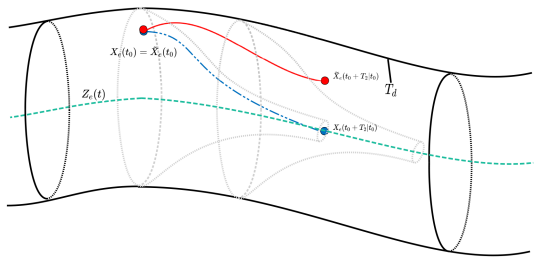

Fig. 1. Illustration: The green line represents the state Z_e of (25). The blue line represents the predicted state of (33). The red line represents the disturbed state of (16). The black line represents the tube centered on the state of system (25). The gray line represents constraints tightening (36).

For the sake of subsequent expression, $E(t) = \begin{bmatrix} S(t) & \gamma(t) \end{bmatrix}^{\mathrm{T}}$. The cost of the ancillary optimization problem is defined as

$$J_2(t_0, X_e(t_0), U_e(t_0)) = \int_{t_0}^{t_0+T_2} l'(X_e(s) - \bar{Z}_e(s), U_e(s), E(s))ds \tag{30}$$

where $T_2 = N_2\delta$, N_2 is the prediction horizon of ancillary controller, $l'(X_e - \bar{Z}_e, U_e, E) = (X_e - \bar{Z}_e)^{\mathrm{T}}Q'(X_e - \bar{Z}_e) + U_e^{\mathrm{T}}R'U_e + E^{\mathrm{T}}P'E$ with $Q' > 0$, $R' \geq 0$ and $P' > 0$. Due to the change in selecting the reference trajectory, the predicted horizon of the ancillary controller should not exceed that of the nominal controller, i.e., $T_2 \leq T_1$.

Assumption 1: This exist local Lipschitz constants L_x and L_ω, such that

$$\|f_e(x_1, u, \omega) - f_e(x_2, u, 0)\|_{\bar{Q}} \leq L_x\|x_1 - x_2\|_{\bar{Q}} + L_\omega\|\omega\| \tag{31}$$

holds for $x \in \mathbb{X}_e$ and all $u \in \mathbb{U}_e$.

Problem 2: The current error state $X_e(t_0)$, reference state trajectory $\bar{Z}_e(\cdot)$ and $S(t_0)$ are given, respectively, the proposed ancillary optimization problem is described as follows:

$$\min_{U_e} J_2(t_0, X_e(t_0), U_e(t_0)) \tag{32}$$

$$\text{s.t.} \quad \dot{X}_e(t) = f_e(X_e(t), U_e(t)),\ t \in [t_0,\ t_0 + T_2] \tag{33}$$

$$\dot{S}(t) = \gamma(t),\ t \in [t_0,\ t_0 + T_2] \tag{34}$$

$$S(t) \leq \bar{S}(t), \gamma(t) \leq \bar{\gamma}(t),\ t \in [t_0,\ t_0 + T_2] \tag{35}$$

$$\|X_e(t) - \bar{Z}_e(t|t_0)\|_{\bar{Q}} \leq S(t) - \mu(t),\ t \in [t_0,\ t_0 + T_2] \tag{36}$$

$$X_e(t) \in \mathbb{X}_e,\ t \in [t_0,\ t_0 + T_2] \tag{37}$$

$$U_e(t) \in \mathbb{U}_e,\ t \in [t_0,\ t_0 + T_2] \tag{38}$$

$$X_e(t_0 + T_2) \in \mathbb{X}_f \tag{39}$$

where $\mu(t) = L_\omega\|\bar{\omega}\|(t - t_0)e^{L_x(t-t_0)}$, the specific expressions for $\bar{S}(t)$ and $\bar{\gamma}(t)$ are given in (51) and (53), respectively. $\|X_e(t) - \bar{Z}_e(t|t_0)\|_{\bar{Q}} \leq S(t) - \mu(t)$ is the constraint tightening as shown in Fig. 1. $\mathbb{X}_e = \{X_e | \|X_e - \bar{Z}_e(t_0 + T_2|t_0)\|_{\bar{Q}} \leq c\}$, $c > 0$, represents a neighborhood near the $\bar{Z}_e(t_0 + T_2|t_0)$, as detailed in *Remark 3*. $\mathbb{U}_e$ is an input constraint, as detailed in (18). There is no terminal cost and only one state in the terminal constraint set

$$\mathbb{X}_f = \left\{\bar{Z}_e(t_0 + T_2|t_0)\right\}.$$

Solving *Problem 2* yields $\bar{U}_e(t)$, $t \in [t_0,\ t_0 + T_2]$, as the optimal control sequence. The value of $\bar{U}_e(t)$ at the first sampling period serves as the control input $\tilde{\kappa}_N(t)$ applied to (16), $\tilde{\kappa}_N(t) = \bar{U}_e(t)$, $t \in [t_0,\ t_0 + \delta]$. The closed-loop system is established as follows:

$$\dot{\tilde{X}}_e(t) = f_e(\tilde{X}_e(t), \tilde{\kappa}_N(t), \omega(t)) \tag{40}$$

where $\tilde{X}_e(t)$ represents the disturbed state affected by disturbances $\omega(t)$ and obtained by applying input $\tilde{\kappa}_N(t)$.

Remark 3: The set $\mathbb{X}_e = \{X_e | \|X_e - \bar{Z}_e(t_0 + T_2|t_0)\|_{\bar{Q}} \leq c\}$ represents a neighborhood near $\bar{Z}_e(t_0 + T_2|t_0)$. Actually, this set must satisfy the condition that, while adhering to the input constraints, at time $t_0 + T_2$, the state $X_e(t + T_2|t_0)$ reaches the terminal set $\mathbb{X}_f$, i.e., $\mathbb{X}_e \subseteq \hat{\mathbb{X}}_e, \hat{\mathbb{X}}_e = \{X_e(t_0) | U_e(t) \in \mathbb{U}_e, X_e(t_0 + T_2|t_0) \in \mathbb{X}_f, t \in [t_0, t_0 + T_2]\}$.

Definition 1: [28] If there exist a $\mathcal{KL}$ function $\beta(\cdot, \cdot)$ and a $\mathcal{K}$ function $o(\cdot)$ such that

$$\|X_e(t)\| \leq \beta(\|X_e(t_0)\|, t) + o(S(t)) \quad t \in [t_0, \infty) \tag{41}$$

where t_0 is the initial time, $S(t)$ represents the distance parameter of the tube, then the closed-loop system (40) is ISS.

Theorem 2: For the closed-loop system (40), suppose that *Assumption 1* holds. Given $Q' > 0, R' \geq 0, P' > 0$, and the reference state trajectory $\bar{Z}_e(t), t \in [t_0, t_0 + T_2]$. If $X_e(t_0) \in \mathbb{X}_e$, then *Problem 2* is feasible and the closed-loop system (40) is ISS for all $t \geq t_0$.

Proof: Considering the existence of terminal constraint (39) and there is only one element in the terminal set $\mathbb{X}_f$, the stability of (40) is directly affected by the terminal constraint. In *Theorem 1*, it is proved that system (25) is asymptotically stable, which implies that $Z_e(t) \to 0$ for $t \to \infty$. So the system $\dot{X}_e(t) = f_e(X_e(t), \tilde{\kappa}_N(t))$ is also asymptotically stable, which implies that there exists a $\mathcal{KL}$ function $\beta(\cdot, \cdot)$ such that

$$\|X_e(t)\| \leq \beta(\|X_e(t_0)\|, t) \quad t \in [t_0,\ \infty). \tag{42}$$

Measuring the influence of disturbances is essential to tighten constraints effectively. Based on *Assumption 1*, we have

$$\begin{aligned} &\|\tilde{X}_e(t) - X_e(t)\|_{\bar{Q}} \\ &= \|\int_{t_0}^{t} f_e(\tilde{X}_e(s), U_e(s), \omega(s)) - f_e(X_e(s), U_e(s))ds\|_{\bar{Q}} \\ &\leq \int_{t_0}^{t} L_\omega\|\omega(s)\| + L_x\|\tilde{X}_e(s) - X_e(s)\|_{\bar{Q}}ds \\ &\leq \int_{t_0}^{t} L_x\|\tilde{X}_e(s) - X_e(s)\|_{\bar{Q}} + L_\omega\|\bar{\omega}\|ds. \end{aligned} \tag{43}$$

Taking the derivative with respect to both sides yields

$$\frac{\mathrm{d}\|\tilde{X}_e(t) - X_e(t)\|_{\bar{Q}}}{\mathrm{d}t} \leq L_x\|\tilde{X}_e(t) - X_e(t)\|_{\bar{Q}} + L_\omega\|\bar{\omega}\|. \tag{44}$$

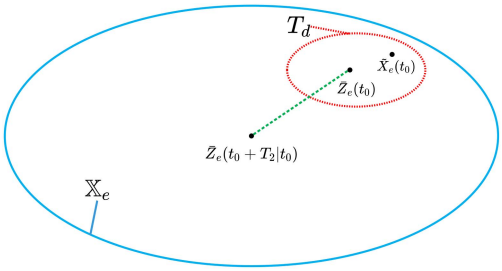

Fig. 2. Illustration: The blue line represents the set $\mathbb{X}_e$. The red line represents the tube T_d. The green line represents the distance between $\bar{Z}_e(t_0+T_2|t_0)$ and $\bar{Z}_e(t_0)$.

Solving the above equation and substituting $\|\tilde{X}_e(t_0) - X_e(t_0)\|_{\bar{Q}} = 0$, we obtain

$$\|\tilde{X}_e(t) - X_e(t)\|_{\bar{Q}} \le L_\omega \|\bar{\omega}\|(t-t_0)e^{L_x(t-t_0)}. \tag{45}$$

Combining this inequality with (36), we have

$$\|X_e(t) - \bar{Z}_e(t)\|_{\bar{Q}} \le S(t) - L_\omega \|\bar{\omega}\|(t-t_0)e^{L_x(t-t_0)}. \tag{46}$$

By adding (45) and (46) and applying the triangle inequality, we obtain that

$$\|\tilde{X}_e(t) - \bar{Z}_e(t)\|_{\bar{Q}} \le S(t). \tag{47}$$

The significance of (47) in the fact that if $X_e(t_0) \in T_d(t_0, \bar{Z}_e(t_0), S(t_0))$, then $X_e(t) \in T_d(t, \bar{Z}_e(t), S(t))$, $t \in [t_0, \infty)$, for all admissible disturbance. Since $S(t)$ has an upper bound $\bar{S}(t)$, combination of (42), there exist a $\mathcal{KL}$ function $\beta(\cdot,\cdot)$ and a $\mathcal{K}$ function $o(\cdot)$ such that

$$\|X_e(t)\| \le \beta(\|X_e(t_0)\|, t) + o(S(t)) \quad t \in [t_0, \infty). \tag{48}$$

Therefore, the closed-loop system (40) is ISS.

Next, we demonstrate the feasibility of *Problem* 2. As shown in Fig. 2, we need to prove that the tube remains within the feasible region of *Problem* 2 at all times, i.e., $T_d \in \mathbb{X}_e$. First, a suboptimal state trajectory is defined as follows:

$$Z'_e(t+T_2|t_0) = \begin{cases} \bar{Z}_e(t+T_2|t_0) & t \in [t_0,\ t_0+T_1-T_2] \\ \hat{Z}_e(t+T_2|t_0) & t \in (t_0+T_1-T_2,\ t_0+T_2]. \end{cases} \tag{49}$$

Since $\bar{Z}_e(t_0+T_1|t_0) \in \mathbb{Z}_f$, $\hat{Z}_e(t+T_2|t_0)$ can be obtained through the linear feedback control law V_e^L. Based on the characteristics of the suboptimal solution, we can obtain

$$\|\bar{Z}_e(t+T_2|t) - \bar{Z}_e(t)\|_{\bar{Q}} \le \|Z'_e(t+T_2|t_0) - \bar{Z}_e(t|t_0)\|_{\bar{Q}}. \tag{50}$$

Therefore, the upper bound of $S(t)$ can be defined as

$$\bar{S}(t) = c - \|Z'_e(t+T_2|t_0) - \bar{Z}_e(t|t_0)\|_{\bar{Q}}. \tag{51}$$

If condition (51) is satisfied, we have

$$\begin{aligned} S(t) &\le \bar{S}(t) \\ &\le c - \|Z'_e(t+T_2|t_0) - \bar{Z}_e(t|t_0)\|_{\bar{Q}} \\ &\le c - \|\bar{Z}_e(t+T_2|t) - \bar{Z}_e(t)\|_{\bar{Q}}. \end{aligned} \tag{52}$$

Algorithm 1: Tube-Based MPC.

1: Initialization:
- The tracking path p_m is given, and the error model (11) and (16) are obtained according to the tracking path and the AUV model.
- Find the appropriate parameters L_x and L_ω based on *Assumption 1*.
- Given the initial time $t_0 = 0$, $S(t_0) = 0$ and $X_e(t_0) = Z_e(t_0)$.

2: Obtain the current nominal state $Z_e(t_0)$, given $Q, R, \mathbb{Z}_e, \mathbb{V}_e$, and $\mathbb{Z}_f$. Solve *Problem 1* and get the nominal trajectory $\bar{Z}_e(t|t_0)$, $t \in [t_0, t_0+T_1]$.

3: Obtain the current actual state $\tilde{X}_e(t_0)$ and $S(t_0)$, given $Q', R', \mathbb{X}_e$ and $\mathbb{U}_e$. With the $\bar{Z}_e(t|t_0)$, $t \in [t_0, t_0+T_1]$ obtained from *Problem 1*, we get $\mathbb{X}_f = \{\bar{Z}_e(t_0+T_2|t_0)\}$. Solve *Problem 2* to obtain $\tilde{\kappa}_N(t_0)$. Calculate the thrust $\boldsymbol{\tau}(t_0)$ through (10).

4: Using the zero-order hold, apply the input $\boldsymbol{\tau}(t_0)$ in the sampling interval $[t_0, t_0+\delta]$.

5: Set $t_0 = t_0 + \delta$ and go back to 2.

Finally, we obtain $\|\bar{Z}_e(t+T_2|t) - \bar{Z}_e(t)\|_{\bar{Q}} + S(t) \le c$, which implies that $T_d \in \mathbb{X}_e$. Let $\bar{\gamma}(t)$ denote the upper bound of γ

$$\bar{\gamma}(t) = \dot{\mu}(t) = L_\omega \|\bar{\omega}\|(1 + L_x(t-t_0))e^{L_x(t-t_0)}. \tag{53}$$

By integrating both sides of (53) from t_0 to t and combining it with (51), we can obtain

$$\begin{aligned} S(t) &\le S(t_0) + \mu(t) - \mu(t_0) \\ &\le c - \|Z'_e(t+T_2+\delta|t_0) - \bar{Z}_e(t+\delta|t_0)\|_{\bar{Q}}. \end{aligned} \tag{54}$$

Since $\mu(t_0) = 0$, we finally obtain

$$\mu(t) \le c - \|Z'_e(t+T_2+\delta|t_0) - \bar{Z}_e(t+\delta|t_0)\|_{\bar{Q}} - S(t_0) \tag{55}$$

where $\mu(t) = L_\omega \|\bar{\omega}\|(t-t_0)e^{L_x(t-t_0)}$. This expression implies the existence of the upper bound $\bar{\omega}$ that satisfies (55).

Hence, the proof is complete. ■

The tube-based trajectory tracking control will be implemented in the receding horizon fashion and the control algorithm is summarized in **Algorithm** 1.

Remark 4: Although solving two optimization problems may take more time than classical tube-based MPC, it should be noted that when the reference state Z_e is zero, solving *Problem* 1 takes almost no additional time as the optimal input sequence V_e, state trajectory Z_e, and cost function J_1 are all zero. The majority of computation time is spent on *Problem* 2.

Remark 5: The approach of addressing the stability of nonlinear systems by using an alternative optimization problem as a replacement for linear feedback was proposed in [31]. Compared to [31], our work differs in several key aspects. First, we incorporate the concept of tightening constraints (36), which allows for more effective control in the presence of disturbances. Second, we explicitly characterize the shape $\bar{Q}$ and size $S(t)$ of the tube, providing a clear understanding of its properties. Finally, we

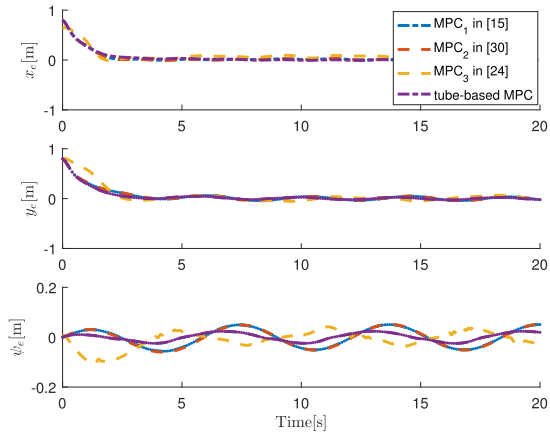

Fig. 3. Tracking errors in x, y and ψ dimensions with different control algorithms in the presence of disturbance ω_1.

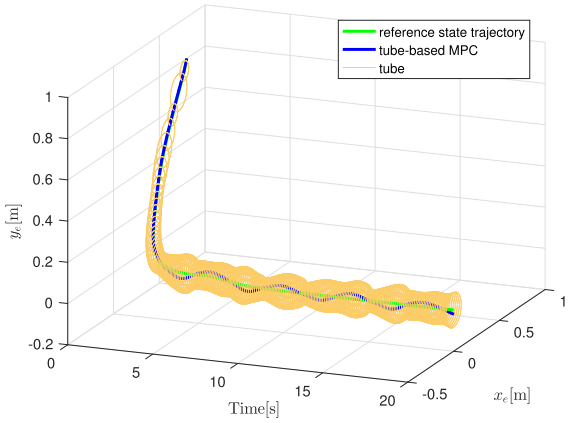

Fig. 4. Real state stay in the tube centered around the reference state trajectory in the presence of disturbances ω_1.

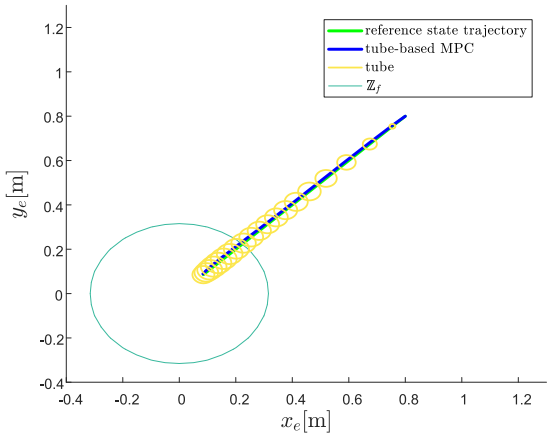

Fig. 5. State transitions from the initial state to the terminal set under the influence of disturbance ω_1.

perform online optimization of the tube-related parameters $S(t)$ and $\gamma(t)$. These differences highlight the contributions of our work in the field of tube-based MPC.

V. Simulation Results

A. Parameter Selection

In this article, we adopt the same AUV model parameters with [15]. And in particular, $M_x = 283.6$ kg, $M_y = 593.2$ kg, and $M_\psi = 29.0\,\text{kgm}^2$. $F_{u,\max} = -F_{u,\min} = 2000(\text{N})$, $F_{v,\max} = -F_{v,\min} = 2000(\text{N})$, and $F_{r,\max} = -F_{r,\min} = 1000(\text{Nm})$. The desired path $x_m(t) = t$ and $y_m(t) = \sin(t)$. The sampling interval $\delta = 0.1$ s. In the *Reference trajectory*, we select prediction horizon $T_1 = 7\delta$, $Q = \mathbf{I}_6$, $R = 0.1\mathbf{I}_3$, and $\sigma = 0.33$. $V_e^L = KZ_e$ and $K = \text{diag}(0.5, 0.5, 0.5, -1, -1, -1)$. In the *Ancillary trajectory*, we select prediction horizon $T_2 = 7\delta$, $Q' = \mathbf{I}_6$, $R' = 0.1\mathbf{I}_3$, $\bar{Q} = \mathbf{I}_6$, and $P = \text{diag}(0.8, 0.2)$. $L_x = 1.8$, $L_\omega = 0.001$. The values of $\bar{S} = 2$ and $\bar{\gamma} = 0.1$ chosen here are conservative to reduce the computational burden. The initial state $X_e(0) = \begin{bmatrix}0.8 & 0.8 & 0 & 0 & 0 & 0\end{bmatrix}^{\text{T}}$.

B. Tracking Performance Under Different Disturbances

To assess the effectiveness of the improved tube-based MPC algorithm, we tested tracking errors under different disturbances (state-independent disturbances and state-dependent disturbances) and compared it with other MPC algorithms. The blue curve MPC_1 corresponds to the algorithm proposed in [15]. The red curve MPC_2 corresponds to the algorithm proposed in [31]. The yellow curve MPC_3 corresponds to the algorithm proposed in [25]. The blue curve tube-based MPC is the improved tube-based MPC implementation. 1) State-independent disturbances In this part, the state-independent disturbance is chosen as $\omega_1 = [90\cos(0.15t)\sin(0.1t) \quad 250\sin(0.15t)\cos(0.1t) 10\cos(0.1t)]$ from the initial time, $\alpha = 0.95$. Fig. 3 shows the tracking errors for various MPC algorithms. In case of external disturbances ω_1, we observe that each of the MPC controller drive the AUV to converge in a bounded region. However, the tube-based MPC has smaller tracking errors. As depicted in Figs. 4 and 5, the real state stay in the tube centered around the reference state trajectory in case of disturbances ω_1. There are roughly two stages to the process: 1) the approach stage; and 2) the arrival stage. The approach stage refers to reaching the terminal set $\mathbb{Z}_f$ from the initial position $X_e(t_0)$, $t \in [0\text{ s}, 2.0\text{s}]$. The arrival stage refers to the terminal set, $t \in [2.0\text{s}, 20\text{s}]$. The control signals are illustrated in Fig. 6, every calculated thrust takes values that are within the allowed range.

2) State-dependent disturbances

In this part, the state-dependent disturbance is chosen as

$$\omega_2 = \begin{bmatrix} -80v^2 + 180\cos(0.15t)\sin(0.1t) \\ -300ur + 500\sin(0.15t)\cos(0.1t) \\ 10ur + 5v^3 + 20\cos(0.1t) \end{bmatrix}$$

from the initial time, $\alpha = 0.8$. Compared to ω_1, ω_2 incorporates variables that are related to the current state. The tracking errors in the presence of disturbances ω_2 are illustrated in Fig. 7. After increasing the disturbance, the states converge to a large region, but tube-based MPC shows better performance than MPC_1,

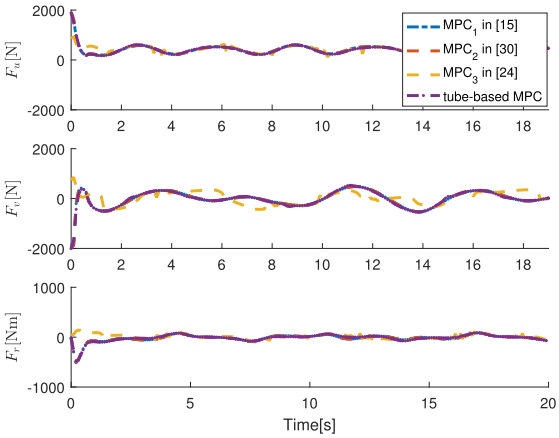

Fig. 6. Control signals with different control algorithms in the presence of disturbance ω_1.

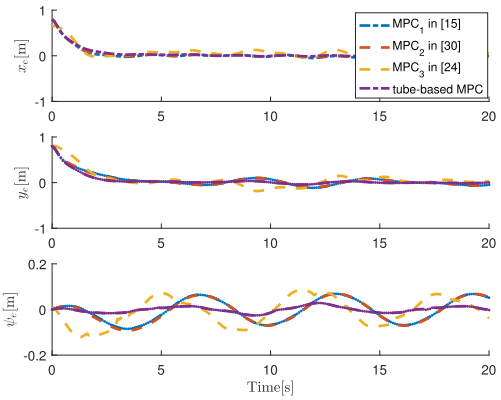

Fig. 7. Tracking errors in x, y and ψ dimensions with different control algorithms in the presence of disturbance ω_2.

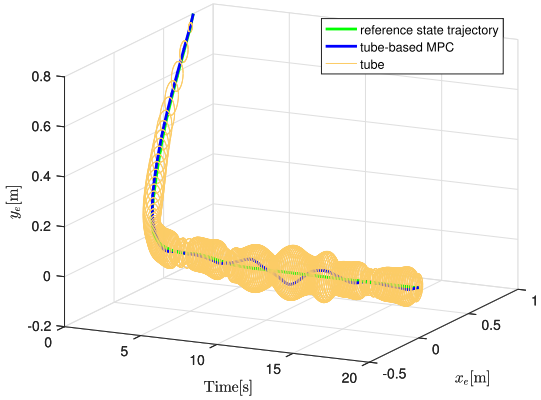

Fig. 8. Real state stay in the tube centered around the reference state trajectory in the presence of disturbances ω_2.

MPC$_2$, and MPC$_3$. In comparison to Figs. 4 and 5, Figs. 8 and 9 illustrate a larger tube in the case of stronger disturbances ω_2. This suggests that the algorithm will exhibit different convergence performances when facing different disturbances, and the tube will also adjust accordingly. The control signals are illustrated in

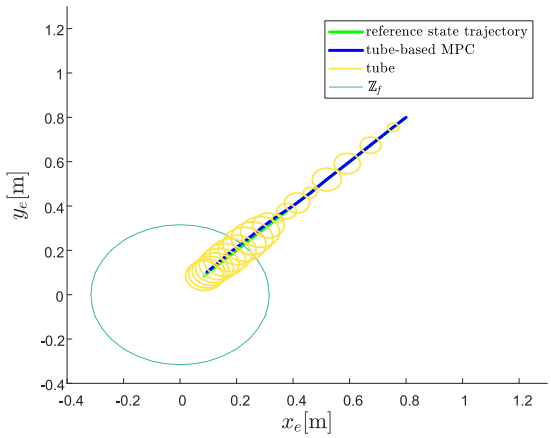

Fig. 9. State transitions from the initial state to the terminal set under the influence of disturbance ω_2.

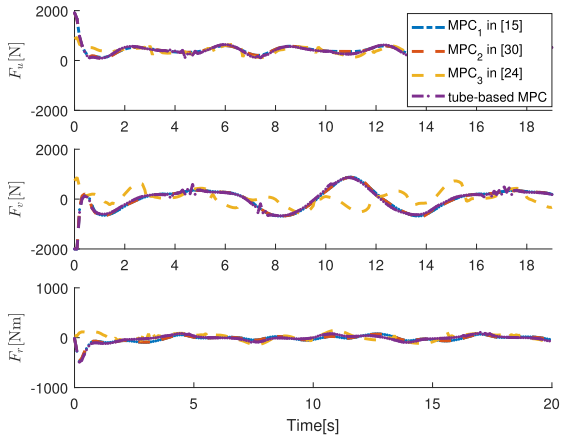

Fig. 10. Control signals with different control algorithms in the presence of disturbance ω_2.

Fig. 10. It should be emphasized that F_u, F_v, and F_r appear some flutter, since the maximum number of iteration $iter_{\max} = 3000$. This implies the calculated value is not necessarily the optimal value when the number of iteration $iter = iter_{\max}$.

VI. Conclusion

This article has developed an improved tube-based MPC of AUVs with an additive bounded disturbance. An error dynamics model is derived from the AUV dynamics and the reference trajectory. The optimization problem was constructed by the error dynamics model. The controller's solution was broken up into two sections. First, the nominal system's *Problem* 1 has been solved to produce a central path. Next, by *Problem* 2 for the disturbed system, we obtained the actual state trajectory, which was located in the tube centered on central path. We determined the shape of the tube offline, added the tube-related tightening constraints to *Problem* 2. The feasibility has been guaranteed if the system state has been in the initial set. The simulation results have illustrated that the closed-loop system is ISS in the presence of bounded external disturbances. In the near future,

to mitigate the conservativeness of handling disturbances solely through upper bounds, we are interested in the integration of stochastic MPC and tube-based MPC approaches.

REFERENCES

[1] T. I. Fossen, *Marine Control Systems–Guidance. Navigation, and Control of Ships, Rigs and Underwater Vehicles*. Trondheim, Norway: Marine Cybernetics, 2002.

[2] Z. Peng, J. Wang, D. Wang, and Q. Han, "An overview of recent advances in coordinated control of multiple autonomous surface vehicles," *IEEE Trans. Ind. Inform.*, vol. 17, no. 2, pp. 732–745, Feb. 2021.

[3] K. Shojaei and M. Dolatshahi, "Line-of-sight target tracking control of underactuated autonomous underwater vehicles," *Ocean Eng.*, vol. 133, pp. 244–252, 2017.

[4] A. Singh, S. Chatterjee, and R. Thakur, "Design of tracking of moving target using PID controller," *Int. J. Eng. Trends Technol.*, vol. 15, pp. 403–406, 2014.

[5] M. Triantafyllou and M. Grosenbaugh, "Robust control for underwater vehicle systems with time delays," *IEEE J. Ocean. Eng.*, vol. 16, no. 1, pp. 146–151, Jan. 1991.

[6] L. Hao, Y. Yu, T. Li, and H. Li, "Quantized output-feedback control for unmanned marine vehicles with thruster faults via sliding-mode technique," *IEEE Trans. Cybern.*, vol. 52, no. 9, pp. 9363–9376, Sep. 2022.

[7] X. Xiang, L. Lapierre, and B. Jouvencel, "Smooth transition of AUV motion control: From fully-actuated to under-actuated configuration," *Robot. Auton. Syst.*, vol. 67, pp. 14–22, 2015.

[8] J. B. Rawlings, D. Q. Mayne, and M. Diehl, *Model Predictive Control: Theory, Computation, and Design*, vol. 2. Madison, WI, USA: Nob Hill Pub., 2017.

[9] B. Kouvaritakis and M. Cannon, *Model Predictive Control*, vol. 38. Berlin, Germany: Springer, 2016.

[10] W. Y. Choi, S.-H. Lee, and C. C. Chung, "Horizonwise model-predictive control with application to autonomous driving vehicle," *IEEE Trans. Ind. Inform.*, vol. 18, no. 10, pp. 6940–6949, Oct. 2022.

[11] Y. Shi and K. Zhang, "Advanced model predictive control framework for autonomous intelligent mechatronic systems: A tutorial overview and perspectives," *Annu. Rev. Control*, vol. 52, pp. 170–196, 2021.

[12] Y. Zhang, X. Liu, M. Luo, and C. Yang, "MPC-based 3-D trajectory tracking for an autonomous underwater vehicle with constraints in complex ocean environments," *Ocean Eng.*, vol. 189, 2019, Art. no. 106309.

[13] W. Gan, D. Zhu, and D. Ji, "QPSO-model predictive control-based approach to dynamic trajectory tracking control for unmanned underwater vehicles," *Ocean Eng.*, vol. 158, pp. 208–220, 2018.

[14] R. V. Parys, M. Verbandt, J. Swevers, and G. Pipeleers, "Real-time proximal gradient method for embedded linear MPC," *Mechatronics*, vol. 59, pp. 1–9, 2019.

[15] C. Shen, Y. Shi, and B. Buckham, "Integrated path planning and tracking control of an AUV: A unified receding horizon optimization approach," *IEEE ASME Trans. Mechatron.*, vol. 22, no. 3, pp. 1163–1173, Jun. 2017.

[16] C. Shen, Y. Shi, and B. Buckham, "Trajectory tracking control of an autonomous underwater vehicle using Lyapunov-based model predictive control," *IEEE Trans. Ind. Electron.*, vol. 65, no. 7, pp. 5796–5805, Jul. 2018.

[17] W. Zheng and B. Zhu, "Control Lyapunov-barrier function based model predictive control for stochastic nonlinear affine systems," *Int. J. Robust Nonlinear Control*, early access, Sep. 2023, doi: 10.1002/rnc.6962.

[18] D. Wang, Q. Pan, Y. Shi, J. Hu, and C. Zhao, "Efficient nonlinear model predictive control for quadrotor trajectory tracking: Algorithms and experiment," *IEEE Trans. Cybern.*, vol. 51, no. 10, pp. 5057–5068, Oct. 2021.

[19] X. Ping, J. Hu, T. Lin, B. Ding, P. Wang, and Z. Li, "A survey of output feedback robust MPC for linear parameter varying systems," *IEEE/CAA J. Automatica Sinica*, vol. 9, no. 10, pp. 1717–1751, Oct. 2022.

[20] D. Q. Mayne, "Model predictive control: Recent developments and future promise," *Automatica*, vol. 50, no. 12, pp. 2967–2986, 2014.

[21] H. Wei, K. Zhang, and Y. Shi, "Self-triggered min-max DMPC for asynchronous multiagent systems with communication delays," *IEEE Trans. Ind. Inform.*, vol. 18, no. 10, pp. 6809–6817, Oct. 2022.

[22] D. A. Allan, C. N. Bates, M. J. Risbeck, and J. B. Rawlings, "On the inherent robustness of optimal and suboptimal nonlinear MPC," *Syst. Control. Lett.*, vol. 106, pp. 68–78, 2017.

[23] R. D. Mcallister and J. B. Rawlings, "Inherent stochastic robustness of model predictive control to large and infrequent disturbances," *IEEE Trans. Autom. Control*, vol. 67, no. 10, pp. 5166–5178, Oct. 2022.

[24] P. R. B. Monasterios and P. A. Trodden, "Model predictive control of linear systems with preview information: Feasibility, stability, and inherent robustness," *IEEE Trans. Autom. Control*, vol. 64, no. 9, pp. 3831–3838, Sep. 2018.

[25] H. Wei, C. Shen, and Y. Shi, "Distributed Lyapunov-based model predictive formation tracking control for autonomous underwater vehicles subject to disturbances," *IEEE Trans. Syst. Man Cybern. Syst.*, vol. 51, no. 8, pp. 5198–5208, Aug. 2021.

[26] S. Heshmati-Alamdari, G. C. Karras, P. Marantos, and K. J. Kyriakopoulos, "A robust predictive control approach for underwater robotic vehicles," *IEEE Trans. Control Syst. Technol.*, vol. 28, no. 6, pp. 2352–2363, Nov. 2020.

[27] H. Zheng, J. Wu, W. Wu, and Y. Zhang, "Robust dynamic positioning of autonomous surface vessels with tube-based model predictive control," *Ocean Eng.*, vol. 199, 2020, Art. no. 106820.

[28] F. Bayer, M. Bürger, and F. Allgöwer, "Discrete-time incremental ISS: A framework for robust NMPC," in *Proc. Eur. Control Conf.*, 2013, pp. 2068–2073.

[29] J. Köhler, R. Soloperto, M. A. Müller, and F. Allgöwer, "A computationally efficient robust model predictive control framework for uncertain nonlinear systems," *IEEE Trans. Autom. Control*, vol. 66, no. 2, pp. 794–801, Feb. 2021.

[30] M. Mirshams and M. Khosrojerdi, "Attitude control of an underactuated spacecraft using quaternion feedback regulator and tube-based MPC," *Acta Astronautica*, vol. 132, pp. 143–149, 2017.

[31] D. Q. Mayne, E. C. Kerrigan, E. V. Wyk, and P. Falugi, "Tube-based robust nonlinear model predictive control," *Int. J. Robust Nonlinear Control*, vol. 21, no. 11, pp. 1341–1353, 2011.

Li-Ying Hao (Member, IEEE) was born in Jilin, China. She received the M.S. and Ph.D. degrees in control science and engineering from Northeastern University, Shenyang, China, in 2008 and 2013, respectively.

From 2013 to 2016, she was with the College of Information Engineering, Dalian Ocean University, Dalian, China. From July 1, 2015 to August 31, 2015, she was a Visiting Scholar with the Department of Electrical Engineering, Yeungnam University, Kyongsan, South Korea. In 2017, she joined Dalian Maritime University, Dalian, China, and she is currently a Professor with the Department of Automation, Dalian Maritime University. From September 2019 to September 2020, she was a Visiting Scholar with the Department of Mechanical Engineering, University of Victoria, British Columbia, Canada. Her current research interests include robust fault-tolerant control, model predictive control, sliding mode control, and deep learning with an emphasis on applications in marine vehicles.

Dr. Hao was an Honoree of Outstanding Young Talents in Dalian, China, in 2022.

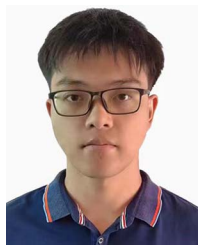

Run-Zhi Wang received the B.S. degree in automation from the University of Science and Technology Liaoning, Anshan, China, in 2021. He is currently working toward the Ph.D. degree in control science and engineering with Dalian Maritime University, Dalian, China.

His current research interests include robust control, sliding mode control, and MPC.

Chao Shen (Member, IEEE) received the B.E. degree in automation engineering and the M.Sc. degree in control science and engineering from Northwestern Polytechnical University, Xi'an, China, in 2009 and 2012, respectively, and the Ph.D. degree in mechanical engineering from the University of Victoria, British Columbia, Canada, in 2018.

He was a Postdoctoral Researcher with the Real-time Adaptive Control Engineering Lab, University of Michigan, Ann Arbor, MI, USA. He is currently an Assistant Professor with the Department of Systems and Computer Engineering, Carleton University, Ottawa, ON, Canada. His primary research interests include control theory, machine learning, and optimization, and their applications in robotics systems, mechatronics systems, and industrial processes.

Dr. Shen was the recipient of the 2018 IEEE SMCS Thesis Grant Initiative for his Ph.D. thesis on model predictive control for underwater robotics, and the Natural Science and Engineering Research Council of Canada (NSERC) Postdoctoral Fellowship in 2020. He was the Associate (Guest) Editor for Special Issues in *IET Control Theory and Applications, Frontiers in Control Engineering*, and in *Journal of Marine Science and Engineering*.

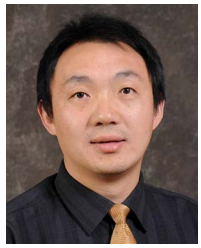

Yang Shi (Fellow, IEEE) received the B.Sc. and Ph.D. degrees in mechanical engineering and automatic control from Northwestern Polytechnical University, Xi'an, China, in 1994 and 1998, respectively, and the Ph.D. degree in electrical and computer engineering from the University of Alberta, Edmonton, AB, Canada, in 2005.

From 2005 to 2009, he was an Assistant Professor and Associate Professor with the Department of Mechanical Engineering, University of Saskatchewan, Saskatoon, SK, Canada. In 2009, he joined the University of Victoria, and is currently a Professor with the Department of Mechanical Engineering, University of Victoria, British Columbia, Canada. His current research interests include networked and distributed systems, MPC, cyber-physical systems (CPS), robotics and mechatronics, navigation and control of autonomous systems (AUV and UAV), and energy system applications.

Dr. Shi was the recipient of the University of Saskatchewan Student Union Teaching Excellence Award in 2007, the Faculty of Engineering Teaching Excellence Award in 2012 at the University of Victoria (UVic), the JSPS Invitation Fellowship (short-term) in 2013, the UVic Craigdarroch Silver Medal for Excellence in Research in 2015, the 2017 IEEE TRANSACTIONS ON FUZZY SYSTEMS Outstanding Paper Award, the Humboldt Research Fellowship for Experienced Researchers in 2018, and the CSME Mechatronics Medal and the IEEE Dr.-Ing. Eugene Mittelmann Achievement Award in 2023. He is IFAC Council Member; VP on Conference Activities of IEEE IES, and the Chair of IEEE IES Technical Committee on Industrial Cyber-Physical Systems. He is currently Co-Editor-in-Chief of IEEE TRANSACTIONS ON INDUSTRIAL ELECTRONICS, and Editor-in-Chief of IEEE *Canadian Journal of Electrical and Computer Engineering*, he is also Associate Editor for *Automatica*, IEEE TRANSACTIONS ON AUTOMATIC CONTROL, *Annual Review in Controls*, etc. He is a Distinguished Lecturer of IES. He is a Fellow of ASME, CSME, Engineering Institute of Canada (EIC), Canadian Academy of Engineering (CAE), and a registered Professional Engineer in British Columbia, Canada.